Fluoropolymer Ferroelectrics: Multifunctional Platform for Polar-Structured Energy Conversion

Abstract

Ferroelectric materials are some of the most widely applied material systems in modern society and are constantly generating improved functions with higher efficiencies. Advancements in poly(vinylidene fluoride) (PVDF)-based polymer ferroelectrics provide flexural, coupling-efficient, and multifunctional material platforms for applications that demand portable, lightweight, wearable and durable features. We highlight the recent advances in fluoropolymer ferroelectrics, their energetic cross-coupling effects and emerging technologies, including wearable, highly efficient electromechanical actuators and sensors, electrocaloric refrigeration and dielectric devices. These developments reveal that the molecular and nanostructure manipulations of the polarization-field interactions, through facile defect biasing, could introduce enhancements in the physical effects that would enable possibilities like multisensory and multifunctional wearables for the emerging immersive virtual world and smart systems for a sustainable future.

One-Sentence Summary - A review of recent advances in polymer ferroelectrics for highly efficient and robust electromechanical, electrocaloric, and dielectric applications.

Although functional inorganic materials such as semiconductors, piezoelectrics, and ferroelectrics often have higher performance metrics arising from the crystalline order than polymers, polymers are attractive alternatives because of the ease of fabrication, mechanical robustness, lower weight and cost, and acoustic impedance matching to tissues and water. Ferroelectrics are insulators that exhibit additional internal polarization ordering, called spontaneous polarization P_s, whose direction can be reversed by applying an electric field (Fig. 1A). Piezoelectricity is a linear electromechanical effect in which an applied electric field E can induce changes in the mechanical stress X in a material and vice versa (Fig 1B). Piezoelectrics are used in actuators, transducers, sensors, and solid-state motors (*2*). While not all piezoelectric materials are ferroelectric, ferroelectrics exhibit the strongest piezoelectricity among the known piezoelectrics. Ferroelectrics also find applications in high-permittivity capacitors, nonvolatile memories, and electro-optical devices (*1, 2*).

These effects were first discovered in inorganic materials, and then in polymers. Piezoelectricity in mechanically stretched poly(vinylidene fluoride) (PVDF) was reported by Kawai in 1969 (*3*), and ferroelectricity in the 1970s (*4*). The development of P(VDF-TrFE) in the early 1980s, in which VDF is vinylidene fluoride and TrFE is trifluoroethylene (*5*-*8*), enabled stronger piezoelectricity and ferroelectric responses without the need for mechanical drawing (*9*). These polymer ferroelectrics have found application in commercial products such as wearable sensors, deformable and flexible transducers for medical imaging, and underwater navigation, soft robots, and actuators (*9*).

Polarization in normal ferroelectrics is present as macroscopic domains. Breaking macroscopic polar domains into nanoscale polar regions via defects and dopants transforms a normal ferroelectric into a relaxor ferroelectric that exhibits a large and reversible (hysteresis-free) electric field-induced polarization change over a broad temperature range (Fig. 1C) (*10*). In all ferroelectrics, the direct coupling of the polarization in the material with external stimuli such as mechanical stress X, temperature T, magnetic field, and optical signals is what leads to a myriad of functional properties and applications. Thus, the discovery and development of relaxor ferroelectricity in the late 1990s and early 2000s in defect-modified P(VDF-TrFE) polymers such as P(VDF-TrFE-CFE) (CFE: chlorofluoroethylene) terpolymers created a design paradigm for polymer ferroelectrics with useful properties such as giant electrostriction and a giant electrocaloric effect (ECE) owing to the electric field-induced large and reversible polarization changes between the nonpolar molecular conformations and polar conformation (*11, 12*). Electrostriction is a nonlinear electromechanical effect in which the mechanical strain x and stress X are proportional to the square of the electric field (and polarization) (*13*). Giant electrostriction expands the applications of ferroelectrics to artificial muscles, better-performing soft robots, and many other electromechanical applications. The ECE is the electric field-induced temperature change in a material (Fig. 1D) (*11, 12, 14, 15*). The ECE is attractive for solid-state refrigeration that emits zero greenhouse gas and is compressor free.

The easy fabrication, mechanical robustness, and acoustic impedance matching to tissues and water of these ferroelectric polymers, coupled with advanced manufacturing, have led to developments and potential applications in fiber wearables, flat-panel and flexible air conditioners (ACs), biomedical devices, artificial muscles, soft robots, emissive energy sensing, and imaging.

Several products in wearables, biomedical devices, and soft robots have been commercialized, and others are still under research development(*16-26*).

Cross-Coupling Phenomena

The coupling between polymers' electric and mechanical energies in the form of the piezoelectric effect (*3-9, 16-18, 20, 27*) is the most widely used feature. The piezoelectric effect is a linear electromechanical effect (*1, 28*), where a mechanical strain (x) and stress (X) generate a charge or voltage output and vice versa:

$$D = d\,X \quad \text{and} \quad x = d\,E \qquad (1)$$

where E is the electric field, D ($\approx P$ in ferroelectrics) is the surface charge density (electric displacement), and d is the piezoelectric coefficient. The electromechanical coupling factor k is another key parameter, and k^2 ($= g\,d\,Y$, where g is the piezoelectric voltage coefficient and Y is the elastic modulus) measures the energy conversion efficiency between electric and mechanical forms (*1, 2, 27*).

Electrostriction is another nonlinear electromechanical effect that exists in all insulators, with

$$x = Q\,P^2 \qquad (2)$$

where Q is the electrostrictive coefficient. It has gained increased interest in after the discovery of giant electrostriction in polymer relaxor ferroelectrics (*11, 13, 29*). In ferroelectrics, the piezoelectric effect can be considered to arise from the electrostriction under a remanent polarization bias (*13, 27*).

The cross-coupling between polarization and temperature in insulating dielectrics that possess polar ordering generates the pyroelectric effect (*1, 15*). In simple terms, the pyroelectric effect refers to the polarization change caused by a temperature variation, $(\frac{\partial P}{\partial T})_E$, while the reverse process, *i.e.*, a reversible entropy (S) or temperature (T) change generated by an electric field change, $(\frac{\partial S}{\partial E})_T$, *e.g.*, the ECE, exists in all insulators. The ECE is usually characterized by an electric field-induced isothermal entropy change ΔS and an adiabatic temperature change ΔT. From Landau-Devonshire (L-D) phenomenological theory,

$$\Delta S = - ½ \beta P^2 \qquad (3)$$

in ferroelectrics, where β is a coefficient in L-D theory that characterizes the electrothermal coupling (*15*). In many cases, the two are related as $T\Delta S = C_E \Delta T$, where C_E is the specific heat of the EC material at a constant E (*1, 15*).

The ECE in polymers is a more recent discovery than the piezo- and pyroelectric effects. EC refrigeration is a highly promising solid-state alternative for cooling (*30-32*) that emits zero greenhouse gases and is compressor free, scalable, and compact (*32*). Although the ECE was observed in Rochelle salt in 1930 (33, 34), ECE studies in the last century were performed on inorganic ferroelectrics, where the small ECE observed was not sufficient for practical use (35-37). Only recently has EC polymer research discovered that facile defect modification of PVDF-based relaxor ferroelectric polymers can lead to a giant room-temperature ECE at ultralow electric fields (14, 22, 38, 39).

Polarization responses and coupling to external stimuli

In ferroelectrics, the coupling (interaction) between the polarization and various external stimuli such as mechanical stress X, temperature T, magnetic field B, and light signals is what generates various cross-coupling phenomena (ferroelectrics are multifunctional). Polarization changes in ferroelectrics originate from different sources and processes that generate different cross-coupling phenomena. Although exhibiting a similar polarization change, the domain switching of an antiparallel polar arrangement, which generates very little electromechanical (EM) coupling, is fundamentally distinct from the field-induced polar reorientation in a three-dimensional (3D) polar structure, which produces strong EM coupling (*40*). In addition, nonvolatile memory demands an irreversible P_s arising from the existence of macroscopic polarization domains, whereas giant EC cooling materials were discovered among relaxor polymers, in which the polarization responses arise from highly polar-disordered to ordered phases that exhibit high reversibility and efficiency (Fig. 1D) (22).

In polymer ferroelectrics, the polarization processes occur at molecular, nanoscopic, mesoscopic and macroscopic scales. In the ferroelectric phase (β-phase), chains of the *all-trans* (*tttt*) conformation form a hexagonal crystal structure (Fig. 1E).The polarization change under

electric fields occurs through successive 60-degree dipole rotations (*9*). Here, a 180-degree (y'-direction to y-direction) dipole rotation generates a large polarization change but zero strain. The dipole rotations from the x (60°) and z' (120°) orientations to the y-direction generate both a polarization change and mechanical strain. Bernholc et al. carried out a density functional theory (DFT) calculation of the EM effect realized through these polarization rotations and showed an electrostrain of -1.1% and a small electrostrictive coefficient Q_{33} of -2.9 m^4/C^2, which is nearly the same as the experimentally observed Q_{33} in P(VDF-TrFE) polymers (*27*).

Adding small amounts of defects such as monomers (e.g. CFE), which are bulkier in size than the VDF and TrFE monomers in VDF-TrFE polymer chains, converts the *all-trans* chain conformation of the β-phase to a chain morphology of mixed conformations of all 4 types (Fig. 1F), the proportions of which depend on the CFE content. Including ca. 6 mol% CFE in P(VDF-TrFE) chains eliminates the *all-trans* conformation and converts the polymer into a relaxor that displays a reversible and large polarization change at room temperature. Moreover, the relaxor polymer generates an electroactuation strain of -7% and a $-Q_{33}$ of more than 10 m^4/C^2, indicating that the polarization changes in the relaxor terpolymer are more efficient in EM coupling. This can be understood from the large difference in the polymer chain dimensions between the highly polar *all-trans* bonds and the three other bonds, *e.g.*, *trans-gauche–trans-gauche' (tgtg')*, t_3gt_3g', and 3/1 helix (*tgtgtg* or *tg'tg'tg'*) (Fig. 1F). Switching from these three nonpolar or nearly nonpolar bonds to the *tttt* bonds generates larger electroactuation and a higher $|Q_{33}|$. For example, the conformational change from *3/1 helix* to *tttt* can generate an interchain strain (d_{space}) of ~8% (Fig. 1G).

By replacing a small amount (~2 mol%) of bulky CFE with fluorinated alkyne (FA), which has a smaller monomer size than VDF and TrFE, the relaxor P(VDF-TrFE-CFE-FA) tetrapolymer was displayed a Q_{33} of -40 m^4/C^2, generating large electroactuation at ultralow electric fields (< 50 MV/m), and ultrahigh piezoelectric coefficient and EM coupling at a DC bias as low as 20 MV/m. The tetrapolymer exhibited a diffused critical endpoint transition region at which the energy barriers for switching from nonpolar to polar molecular conformations become small due to the presence of a small number of polar seeds. Thus, a small change in the electric field induces large electroactuation (*41*). A similar enhancement was also observed in the ECE. A giant ECE at an ultralow electric field was observed in P(VDF-TrFE-CFE-FA) relaxor tetrapolymers with only

0.6 mol% FAs. Moreover, the β coefficient in Eq. (2) of the tetrapolymer is 4 times that of P(VDF-TrFE-CFE) (*22*).

The results for these relaxor polymers reveal the critical importance in facile application of molecular dissimilarities and defects to control different polarization processes and tailor barriers for desired polarization switching to generate the desired material performance at high efficiency.

Among polymer ferroelectrics, including nylon-based ferroelectrics and others (*9, 42, 43*), PVDF-based polymers exhibit the best ferroelectric, EM coupling, and electrothermal coupling properties. Moreover, PVDF-based ferroelectric relaxor polymers display the highest reversible room-temperature polarization changes, making them attractive for energy storage and other dielectric applications.

PVDF-Based Ferroelectrics

PVDF and P(VDF-TrFE) copolymers

PVDF is the first known polymer ferroelectric. Copolymerizing VDF with TrFE stabilizes the ferroelectric β phase without drawing, and P(VDF-TrFE) shows a ferroelectric-paraelectric (F-P) transition at more than 18 mol% TrFE (*9, 44*). VDF has a dipole moment of 3.0 Debyes in the β phase. TrFE has a dipole moment of approximately half that of VDF in the β phase; therefore, increasing the amount of TrFE in the copolymers will weaken the ferroelectricity, as reflected by the decrease in the F-P transition temperature with the TrFE content, and at a TrFE content of more than 45 mol%, the F-P transition becomes continuous (*9*). Additionally, P(VDF-TrFE) is a semicrystalline polymer, and the ferroelectricity is from the crystalline phase. While the crystallinity of PVDF is approximately 50%, P(VDF-TrFE) at compositions near 70/30 mol% can reach a crystallinity of over 90%. The copolymers near this composition exhibit the best ferroelectric and EM properties (*9*). In addition to the crystallinity, the crystalline orientation (and mechanical drawing) also has a great influence on ferroelectric and other functional properties (*9, 27, 45*). Moreover, as early as 1998, Bune et al. reported 2D ferroelectrics for Langmuir-Blodgett P(VDF-TrFE) films two molecular layers thick (*46*).

All of these properties make P(VDF-TrFE) a useful material system for developing an understanding of ferroelectricity in polymers. For example, polar topological textures have become

an emerging research field for exotic phenomena and potential application in reconfigurable electronic devices. In 2021, Guo et al. reported a toroidal topological texture self-organized P(VDF-TrFE) copolymer that exhibits a concentric topology with anti-coupled chiral domains (Fig. 1I**)** in spin-coated thin films with polymer chains vertically aligned and a permanent polarization lying along an in-plane direction of the film (*47*). The interplay among the elastic, electric, and gradient energies in the highly strained polymer films results in continuous rotation and toroidal assembly of the polarization perpendicular to polymer chains, whereas relaxor behavior is observed along polymer chains. Moreover, the toroidal polar topology of the films also exhibits the ability to microscopically manipulate terahertz waves, which might find application in terahertz raster scanning and spatial light modulators (*47*).

The piezo d_{ij} coefficients and EM coupling efficiency of PVDF and P(VDF-TrFE) are approximately one order of magnitude lower than those of their ceramic counterparts (Table 1). In ferroelectrics, the morphotropic phase boundary (MPB) is a transition region in the phase diagram bridging two nearly energetically degenerate phases with distinct symmetries, thus lowering the polarization rotation barriers and consequently enhancing the piezoelectric response. In 2018, Liu et al. reported the finding of an MPB in P(VDF-TrFE) copolymers, and the P(VDF-TrFE) copolymers at MPB compositions had a piezoelectric d_{33} of -63.5 pm/V, double that of compositions away from the MPB, albeit still far below the d_{33} of 650 pm/V for the inorganic counterpart (Fig. 1I)(*48*). In contrast to their inorganic counterparts, the d_{33} and Q_{33} of PVDF-based ferroelectric polymers exhibit negative signs due to the chain conformations and crystal structurs of polar and nonpolar phases(*27, 49*).

In contrast to the piezoelectric effect, P(VDF-TrFE) copolymers, which have intrinsic "polar disorder" in the paraelectric phase, should generate a large ECE near the F-P transition. A paraelectric is a dielectric that does not possess polar ordering and transitions to a ferroelectric at certain temperatures or under mechanical stresses. Using Eq. (2), $\Delta S = -\frac{1}{2}\beta P^2$, leads to $\Delta S = 96$ J/(kgK) and $\Delta T = 26$ K at the F-P transition of 100 °C of P(VDF-TrFE) copolymers, orders of magnitude higher than observed in ceramics (*15, 50*). Experimental studies of the ECE in P(VDF-TrFE) near the F-P transition confirmed this in the late 2000s (*14, 51*).

Relaxor ferroelectrics and their nanocomposites

Relaxor ferroelectrics were discovered in the late 1990s, which created a new polymer ferroelectric design paradigm and t offered promising properties in several technological areas (*11, 12, 52, 53*). Incorporating molecular defects such as a small molar percentage of monomers, *e.g.*, CFE and chlorotrifluoroethylene (CTFE), which are bulkier than VDF and TrFE in P(VDF-TrFE) normal ferroelectrics, effectively modulated the crystalline and domain structures and eliminated undesired ferroelectric hysteresis. The broad dielectric transition peak of the resulting relaxor ferroelectric polymer moved to room temperature, with a high dielectric constant K > 50, which is the highest among all known polymers at room temperature, while maintaining a large and reversible polarization change (*11, 12*).

In most EM applications, piezoelectric materials with large electroactuation strains (large shape changes) are highly desired. For ferroelectric polymers, the small piezoelectric coefficients, even under a high electric field of 150 MV/m, limit the electroactuation strain to < -1%. The PVDF-based relaxor polymers were the first among electroactive polymers that generated ultrahigh electroactuation of more than -7% at room temperature (and $\Delta x/\Delta E$ > 400 pm/V), much higher than that of the normal ferroelectric P(VDF-TrFE) (*12, 29*).

A giant ECE was discovered in PVDF-based relaxor polymers at room temperature, *i.e.*, ΔT = 20 K (and ΔS=100 J/(kgK)) in electron-beam-irradiated P(VDF-TrFE) copolymers and ΔT = 16 K (and ΔS=80 (J/kgK)) in P(VDF-TrFE-CFE) terpolymers at an electric field of 150 MV/m (*38, 39*). The relaxor P(VDF-TrFE-CFE) and P(VDF-TrFE-CTFE) terpolymers have been scaled up and are now commercially available from Arkema Piezotech. These EC polymers enabled EC device studies, which demonstrated the potential of EC cooling, especially for wearable, localized, and distributed cooling (*23, 24, 32, 54-56*). The large ECE and wide temperature window rendered the terpolymer an effective base matrix for developing various types of nanocomposites in seeking a larger ECE, better field efficiency, and better overall thermal and mechanical parameters than the neat polymers (*19, 57, 58*). At higher electric fields > 200 MV/m (Table 2), a much larger ECE can be generated in relaxor ferroelectric polymer nanocomposites (*58, 59*).

Polymer relaxors also provide another avenue to study relaxor phenomena. Despite more than five decades of intensive research, polymer relaxors remain one of the least understood material families among ferroelectric materials. Liu et al. showed that the relaxor behavior of ferroelectric polymers originates from conformational disorder, completely different from classic

perovskite relaxors, which are typically characterized by chemical disorder and the presence of nanoscale polar domains *(10, 60).*

Fluorinated alkyne (FA) -defect-modified relaxor ferroelectrics

Although the giant ECE and giant electroactuation in relaxor polymers such as P(VDF-TrFE-CFE) terpolymers have created great interest, a key limitation for applications has been electric breakdown, *e.g.*, the voltage is so high that the device arcs and fails.. The large ECE (Table 2)) and large electrostrain reported are measured near the dielectric breakdown of small samples. For reliable device operation, the applied voltage (and electric field) should be far below the electric breakdown for the materials used in the device. For example, for P(VDF-TrFE-CFE) terpolymers, this limiting field is approximately 60 MV/m. The EC-induced ΔT under this field for the best terpolymers is 3 K (*23, 24, 39*). For caloric refrigeration to provide meaningful cooling, an EC $\Delta T > 5$ K at the limiting field is required (*22-24, 61-63*).

A giant ECE under low electric fields was recently reported in a high-entropy EC polymer. By replacing a small amount (0.6 mol%) of bulky CFE in P(VDF-TrFE-CFE) with double bonds (*i.e.*, FA), the resulting polymer exhibited a large ECE ($\Delta T > 7$ K) under 50 MV/m (Fig. 1J)(*22*). Moreover, no sign of fatigue appeared after 1 million electric cycles (*22*). The simulation results showed that the solid-state refrigerator operating the high-entropy polymer through an active regeneration cycle exhibited a high cooling power density greater than 10 W/cm^3 (and 5 kW/kg) at zero temperature span, T_{span} or a T_{span} of over 50 K at no load (*22, 56*). The simulation results suggested that the EC-based air conditioning/heat pump (AC/HP) system holds the potential to reach a similar refrigeration power/refrigerant charge ratio to that of a VCC-based AC/HP system, which requires 1∼1.6 kg refrigerant charge to offer 5∼6 kW heating and cooling capacity (*64*).

In addition to the FA-modified P(VDF-TrFE-CFE) terpolymers, Goupil et al. reported ECE enhancement for FA-modified P(VDF-TrFE-CTFE), from $\Delta T = 1.3$ K for the pristine terpolymer to $\Delta T > 2$ K with 5 mol% FAs, a 60% enhancement (*65*). The CTFE-based relaxor terpolymer and tetrapolymer generate much smaller ECEs than their CFE-based counterparts, indicating the critical importance of properly designed defects in influencing and controlling the polarization responses of PVDF-based ferroelectric polymers.

Ultrahigh piezoelectricity and EM coupling efficiency were observed in FA-modified P(VDF-TrFE-CFE) at approximately 2 mol% FAs (*27*). Under a low DC bias of 40 MV/m, the mechanically stretched tetrapolymer exhibits an EM coupling factor k_{33} (an indicator of the efficiency of EM energy conversion) of 88% and a piezoelectric coefficient d_{33} of –1050 pm/V (Table 1, Fig. 1K). For the tetrapolymer P(VDF-TrFE-CFE-FA) (63.6/30/4.4/2 mol%), even at a 20 MV/m DC bias, d_{33} = -1177 pm/V and a coupling factor of 71% can still be obtained. These values are higher than those of the most widely used piezoelectric material lead zirconate titanate (PZT). Considering that these tetrapolymer films can be easily made into films below 3 μm thick, the DC bias voltage for 20 MV/m is less than 60 V. Most ferroelectric devices are in the multilayer (ML) film form, which decouples the dielectric layer thickness from the device thickness (*63, 66*). Moreover, approximately 2 mol% FAs in the P(VDF-TrFE-CFE) 68/32/7.3 terpolymer enhanced the electroactuation by more than three times at 60 MV/m compared with the neat terpolymer *(27).*

Electromechanical Applications of PVDF-Based Polymers

PVDF-based ferroelectric polymers have targeted for wearable and implantable mechanical energy harvesters and green energy harvesters since the early 1980s. Examples include an implantable physiological power supply driven by the spontaneous breathing of a dog (*67*) and a PVDF stave inserted beneath the feet for generating electrical energy during walking (*68*). The low acoustic impedance of ferroelectric polymers is well matched to water and tissues and enables efficient power transmission between acoustic and ultrasound transducers and tissues as well as water, which is desirable for sensing and imaging (*16, 69*). For electroactuation, relaxor polymers with an elastic modulus > 0.2 GPa and an actuation strain > 5% at low electric fields (*27*) perform better than ferroelectric ceramics and are better suited for applications that require a large strain and a high force level in free-standing films at low electric fields. Such applications include artificial muscles, soft robots, and haptic feedback.

Energy harvesters and charge generators

Extensive studies have been performed with PVDF-based polymers for energy harvesting (*70-75*). For a piezoelectric energy harvester, the output energy is proportional to the square of the EM coupling factor. To improve the energy harvesting performance, polymer composites with piezoelectric ceramic nanofillers have been shown to be effective. The selection of nanofillers should focus on high-*d* but low-*K* ceramics. For example, a PVDF composite with 5 vol% oriented

$BaTi_2O_5$ nanorods, which has a $K < 100$ and a d_{33} comparable to that of $PbTiO_3$, exhibits twice the peak output power density (0.82 μW/cm^2) than that of neat PVDF (*76*).

Synergy of piezoelectric and triboelectric effects is another effective way to reinforce energy harvesting. The remnant polarization of ferroelectric polymers can effectively strengthen the triboelectric effect, and together with the piezoelectricity of ferroelectrics, Yousry et al. reported an effective piezoelectric charge coefficient $\Delta Q/\Delta F$ = -1065 pC/N and a peak output power density of 0.21 μW/cm^2 at an acceleration of 3G (G=9.8 m/s^2, gravitational acceleration) (*77*).

Polymer fiber wearables

For wearable piezoelectric polymer devices (*74, 78, 79*), PVDF-based polymers can be fabricated into fibers and then into clothing. Electrospun PVDF fibers (*18, 80, 81*) can be easily incorporated into composite materials to further enhance the performance. The surface of nanofillers was proposed to generate electrostatic interactions with PVDF chains that facilitate the formation of the β-phase, thus enhancing the piezoelectric performance. For example, adding both graphene nanosheets and $BaTiO_3$ nanoparticles resulted in a > 90% content of the β-phase of PVDF fibers, which can work as a high-performance flexible piezoelectric nanogenerator (PENG, Fig. 2A) . The device exhibited an output voltage of ~11 V with a maximum electric power of 4.1 μW under a loading frequency of 2 Hz and a strain of 4 mm (*82*).

A bioinspired fabric containing P(VDF-TrFE)/$BaTiO_3$ nanocomposite fibers as acoustic sensors exhibits good performance in sound detection. The nanocomposite fiber exhibits a d_{31} of approximately 45 pC/N (45 pm/V), compared with a value of 20 pC/N for the pure P(VDF-TrFE) fiber (*20*). By mimicking the natural tympanic system (Fig. 2B), a membrane with a combination of high- and low-modulus yarns enables recording of short impulses of acoustic vibrations of only 10^{-7} atmosphere pressure waves. The P(VDF-TrFE) composite fibers on the membrane produce an electrical output that is two orders of magnitude higher than the standalone fibers. The resulting minimum sound detection capability is 0.002 Pa (40 dB, the sound pressure level in a quiet library). A sensitivity of 19.6 mV was measured for the fiber-on-membrane, which is comparable to that of the off-the-shelf condenser and dynamic microphones, for which the values are typically 5 mV (*20*).

An emerging area in which polymer ferroelectrics can play a role are face masks (Fig. 2C), which are key personal protective equipment (PPE) in protecting people from viral infection. The heart of state-of-the-art face masks (e.g. N95) is the electrostatic polypropylene (PP) polymer fiber air filter, which, through surface charges (electrostatic forces), traps (filters) viruses, prevents them from reaching the face and increases the efficiency by several orders of magnitude for the same pressure drop compared with pure mechanical filters. However, the low thermal stability (< 60 °C) of PP electrets limits their shelf and service life. In addition, the surface charge in PP electrets is several orders of magnitude lower than that in PVDF polymers. Indeed, PVDF polymer fiber meshes, through the piezoelectric effect (mechanical motion during breathing) and pyroelectric effect (temperature change during breathing), have been shown to be able to generate a much higher voltage (and charge) than PP electrets (*21*). Furthermore, PVDF fiber meshes can be easily cleaned (disinfected) by washing. In addition to PVDF fiber meshes, the piezoelectric poly(L-lactic acid) (PLLA) filter has also been shown to possess a high filtration efficiency for human breathing, also due to the piezoelectric charge naturally activated by respiration through the mask (*26*).

Ultrasonic imaging

In high-frequency medical and biological ultrasound imaging, P(VDF-TrFE) is extremely useful because of its low acoustic impedance, excellent flexibility, and ability to exhibit stable piezoelectric/dielectric properties in thin films (micrometer scale) (*16*). Commercial instrumentation of high-frequency ultrasound transducers has also been developed in image recognition like the Qualcomm fingerprint scanner. The scanner is constructed by film capacitor field-effect transistors, wherein P(VDF-TrFE) high-density arrays work as the gate dielectric to recognize the pressure with good spatial resolution. The scanner detects three-dimensional details and fingerprint characteristics such as ridges and sweat pores, which cannot be detected with capacitive touch-based and optical options, and has a thin and compact device size (Fig. 2D)(*83*). Such ferroelectric polymer ultrasonic image recognition technology has broad impacts, including for personal IDs, gate access for buildings, smart car ignition, and others by providing higher sensitivity and more detailed biological information.

Soft robotics

The high ductility and easy fabrication in the desired and complicated form enable the use of PVDF-based polymers in soft robotics. Mobility and robustness are two important features for practical applications of robots. Soft robots made of polymeric materials may potentially achieve both attributes simultaneously. Wu et al. reported soft robots based on a curved PVDF unimorph piezoelectric structure, whose relative speed of 20 body lengths per second was one of the fastest reported for artificial insect-scale robots (*17*). The design (Fig. 2E) is inspired by several principles of animal locomotion. Such fast and ultrarobust insect-scale soft robots have potential for application in environmental exploration, structural inspection, information reconnaissance, and disaster relief. The results also showed that the improved piezoelectric performance of the tetrapolymers enables better mobility of soft robots.

Haptic actuators

Emerging virtual and augmented reality technologies are raising the demand for communication between humans and the virtual world, including optical, auditory, and tactile feedback. Haptic technologies enable humans to touch and interact with the contents of virtual environments (*84*). Haptic actuators generate vibrations at frequencies most sensitive for human touch, a few hundred Hz, with a high acceleration of a few *G*s. The large strain (and hence displacement) of the relaxor polymer thin film actuators provides excellent matching to the required haptic actuators. Compared to traditional actuator technologies that rely on piezoceramics, relaxor ferroelectric polymers can generate > 50 times larger strain without mechanical failure. A haptic device commercialized by KEMET with thin film relaxor polymer actuators can generate a 0.2 mm out-of-plane displacement with a 210 V operation voltage (*85*).

Another design for localized tactile feedback was reported by Duong et al. The active layer of the P(VDF-TrFE-CTFE) terpolymer is sandwiched by an electrode and a spacer that separates the layer from touching another electrode (Fig. 2F). The flexible active material and large actuation enable localized tactile feedback. A 200 Hz AC voltage is applied on the electrode. Upon finger pressing, the active layer locally touches the other electrode, resulting in a localized electric field being applied on the terpolymer and triggering its electrostrictive actuation to generate localized vibrational tactile feedback (*25*).

Polymer-Based Electrocaloric Refrigeration

As an EC material reversibly heats up and cools down under electric cycles, a refrigeration cycle, such as the Bryton cycle, can be formed to pump heat from a heat load to a heat sink (*32*). By exploiting the large ECE in commercial relaxor terpolymers, several EC cooling modules have been developed.

Active EC regeneration

Gu et al. reported a series of EC devices (Fig. 3A) that use EC polymers and ceramics fabricated in multilayer capacitor (MLC) structures (*56, 86, 87*). To accumulate the heating and cooling effects at the cold and hot ends of the device and further extend the temperature span of the device, active electrocaloric regeneration (AER) in a polymeric EC device was first demonstrated in 2013 (*56*). A regenerator with anisotropic thermal conductivity was designed and fabricated to minimize the heat loss between the hot and cold ends of the chip-sized device. The device exhibited a 6.6 K temperature span at room temperature and a frequency of 1 Hz, which is comparable to that of the all-solid EC device reported by Wang et al. in 2020 utilizing multilayer ceramic capacitors (MLCCs) (*88*).

An AER device with counterrotating EC disks has also been developed, numerically and experimentally (Fig. 3B) (*86, 89*). In this AER counterrotating disk device design, the inactive heat regeneration layers are eliminated, and instead, the active EC layers stacked in the counterrotating disks serve both the regeneration layers and the active EC working body, thus improving the AER performance. Because of the ease of applying an electric field to the EC unit in the disks, the device geometry can be more sophisticated than that based on magnetocaloric and barocaloric effects (*55, 90*).

In addition to all-solid EC devices, solid–fluid coupling heat exchange was also used to boost efficient heat transfer. By using the commercial EC terpolymer as a cooling core that directly transfers the heat to the reciprocal air flow, the United Technology Research Center (UTRC) reported a heat-exchanger-free "direct air cooing device" (*91*). Different from the design of all-solid EC devices, a device employing fluid–solid contact can dramatically reduce the energy loss from the interface thermal resistance and eliminate the passive heat exchanger (*92, 93*). The prototype developed by the UTRC demonstrated a 14 °C T_{span} at room temperature (Fig. 3C-D)(*91*), which is the highest among all the EC devices (*23, 24, 62, 88, 94, 95*). By ensuring good thermal contact during refrigeration cycling, EC cooling devices were expected to exhibit a large cooling

power (over 1 kW) utilizing a device design of solid–fluid coupling (*54*). Moreover, solid–fluid heat transfer can be realized by designing EC polymeric tubes that exchange heat with the fluid running through them (Fig. 3E-F) (*94*).

Electrostatic EC heat pumps

By integrating the electrostatic force and the ECE, an EC cooler without external motors is possible that enhances the device coefficient of performance (COP). Ma et al. reported a flexible cooling device made of a P(VDF-TrFE-CFE) terpolymer stack, in which the EC polymer film stack oscillates between the cold and hot ends, driven by the electrostatic force (*23*). A cascaded polymeric EC heat pump was developed stacking several cooling units together, which greatly enlarges the temperature span of the heat pump (Fig. 3G)(*24*) and generates cooling of 0.78 W (1,100 W/kg cooling power density) at a 2.7 K temperature rise. The device demonstrated the versatility and feasibility of EC cooling technology in wearable devices for providing localized thermal management (Fig. 3H). A wearable cooler that provides an additional cooling of 4~5 K was shown to be sufficient for personal comfort *(96)*.

Despite the demonstrations of EC devices for compact and wearable cooling, their performance is far from the requirements for practical EC cooling systems (*23, 24, 62, 88*). Owing to the constraints of electric breakdown, the EC temperature change ΔT in all EC devices (including those with ceramics) is below 3 K. This is too small to generate meaningful cooling due to various parasitic thermal losses. In contrast, simulation results show an extrapolated device performance with a high cooling power density of 5 kW/kg at zero T_{span} or a T_{span} of over 50 K at no load for EC coolers with EC P(VDF-TrFE-CFE-FA) tetrapolymers (ΔT=7.5 K) (840 W/kg at zero T_{span} and a T_{span} of over 45 K at zero cooling power with ΔT = 5.5 K for EC ceramics) (*22, 62*).

Dielectric Applications

Flexible nonvolatile memory

For flexible electronics, PVDF-based nonvolatile memories could offer high data storage density and low operation voltage (*97-99*). For example, ferroelectric field-effect transistors (FeFETs) (*100*) and ferroelectric tunnel junctions (FTJs) (*101*) both exhibit longer-lived nondestructive read operations (*102*). A three-terminal memristive device can be created by

replacing the gate dielectric in an FET with P(VDF-TrFE) (*100*). Associated with other flexible components in FETs, a prototype of PVDF-based flexible memory (i.e. an FeFET) , was demonstrated(Fig. 4A). The ON/OFF ratios between data "1" and "0" remain stable even for devices undergoing deformation of <1 mm bending radius or 1000 sharp folding cycles (*98*).

The successful demonstrations of mechanical flexibility in polymer FeFET inspired the development of smart wearable electronics. A rational approach to device integration of PVDF FeFETs into wearable electronics is to fabricate the devices on fibers, followed by the manufacturing of sewn fabrics (Fig. 4B). Stretching the fabric by 100% or crumpling the fabrics will not influence the memory functions (*103*).

In addition to the flexibility of PVDF-based memory, two critical performance parameters await improvement: a high data storage density and a low operation voltage. PVDF-based polymers are thermoplastic materials that are easily shaped at high temperatures. Nanoimprint technologies have been used to fabricate P(VDF-TrFE) nanoarrays with a single storage unit size < 100 nm, exhibiting the possibility of the data storage density reaching several GB/in^2 (*104, 105*). A more practicable design for high-density data storage is vertical 3D stacking of FeFETs (Fig. 4C), in which every single unit can work independently (*106, 107*).

The development of multilevel data storage in which a single memory unit can store more than 2 types ("0" and "1") of data was demonstrated in a PVDF-based FeFET, which also exhibits potential in enhancing the storage density (*106, 108*). By modulating the gate voltage to yield various remnant polarizations of the ferroelectric layers, the semiconductor channels can reflect distinctive resistivities, resulting in multilevel storage features. Moreover, the high transparency of PVDF-based polymer thin films for visible light presents the possibility of combining optical switching of the electrical properties of the semiconductor layer and electrical switching of the ferroelectric polarization of the dielectric layer to realize multifunctional memories with stable multilevel storage features (*109*).

One major disadvantage of using PVDF-based polymers in memory is their high coercive field, ~50 MV/m. Therefore, a nanoscale thin film is required to make the operation voltage match the common operation voltage in integrated circuits. Many studies have reported the existence of ferroelectricity in PVDF-based materials at the nanoscale (*110*), confirming the capability of PVDF-based materials to work as memory in ultrathin films with a low switching voltage. Because

of the ultrathin film of the ferroelectric layer, PVDF-based FTJs exhibit very low operation voltages; for example, Au/P(VDF-TrFE)/ITO FTJ memristor devices can execute "write" and "erase" operations at 0.5 V and -0.4 V, respectively, along with "read" at 0.01 V (*111*).

Energy storage film capacitors

The high polarization together with high breakdown strength of PVDF-based polymers broaden their applications to film capacitors, given that their energy density can be easily higher than 10 J/cc, compared to the value of 5 J/cc for the state-of-art film capacitor with biaxially oriented polypropylene (BOPP) (*112, 113*). This is ideal for capacitor applications that require reduced device size, for example, implantable cardioverter defibrillators (ICDs) (*114*). Several major medical device companies are actively exploring such an option to replace the current tantalum electrolytic capacitors in ICDs. One critical step for dielectric and energy storage applications is to eliminate the polarization hysteresis in PVDF-based ferroelectric polymers and achieve a large and hysteresis-free polarization change.

Cost is another critical consideration for film capacitors. Hence, most studies have focused on PVDF-based copolymers with various defects, such as CTFE and hexafluoropropylene (HFP), which have yielded promising results. Moreover, Ren et al. reported that even in neat PVDF, an ultrahigh discharged energy density, *i.e.,* 50.2 J/cm^3 at 1 GV/m, can be achieved in continuously folded films (Fig. 4D)(*115*). The major challenge of developing practical PVDF-based capacitors is to achieve a delicate balance between a high energy density and a low dielectric loss/low charge carrier conduction. One viable approach is to use ML films of PVDF with a high breakdown strength and a low-loss linear dielectric polymer, such as polycarbonate (PC) and poly(ethylene terephthalate) (PET). By optimizing the composition, layer thicknesses, and interfacial layers, ML film capacitors (Fig. 4E) with high-energy-density (~16 J/cc), low-loss (~0.006), and improved thermal stability (up to 140 °C) have been demonstrated (*116, 117*). Another approach for capacitive energy storage relies on polymer/inorganic nanofiller composites, which use high-K ceramic fillers to enhance the apparent permittivity. Following the mixing rules, this method usually requires a high filler loading (>10 vol%) to obtain a sizable increase in the permittivity. However, the major shortcoming of using nanocomposites is the inevitable aggregation of nanofillers, particularly at high filler loadings, leading to ready dielectric breakdown and mechanical brittleness (*118, 119*). Y. Thakur et al. and T. Zhang et al. reported the discovery of

dilute nanocomposites in which nanofillers at ultralow loadings (< 0.3 vol%) generate large enhancements in both the dielectric constant and electric breakdown strength while maintaining a low dielectric loss in several high-temperature polymers (*120, 121*). An analogous phenomenon is also observed in P(VDF-HFP) copolymers, in which only 0.8 vol.% surface-hydroxylated $Cd_{1-x}Zn_xSe_{1-y}S_y$ nanodots generate a more than 100% enhancement in the dielectric constant together with a slight enhancement in the breakdown strength (*122*).

Conclusion and Outlook

The advances in PVDF-based polymer ferroelectrics from ferroelectric P(VDF-TrFE) in the 1980s to P(VDF-TrFE-CFE-FA) tetrapolymers in the early 2020s demonstrate the promise and impact of molecular and nano- and mesostructure engineering in facile tailoring of the polarization processes to obtain the desired cross-coupling effect and generate the effect(s) at low electric fields. The tetrapolymer results for electrothermal and EM couplings and associated polarization responses reveal an unexplored horizon of polymer ferroelectric research (*22, 27*). The polarization in polymer ferroelectrics originates from different sources and processes over different length scales from molecules to nano- and meso-structure morphologies and micro- and macroscale polarization domains, which endow the materials with multifunctional properties.

For ferroelectric polymers, although dipoles in polymer chains are the key to polarization, dilute nanocomposite phenomena reveal that for the same polymer dipoles, a minute amount of nanofillers (less than 0.2 vol%) can induce local and nanoscale polymer chain morphology changes that lead to marked enhancements in the dielectric constant (and, consequently, polarization) and electric breakdown strength (*120, 121*). In functional materials, employing minute amounts of dopants and defects to tailor, establish, and enhance the desired functional performance is well known and widely used. The advances in PVDF-based polymer ferroelectrics and dilute nanocomposites also demonstrated the effectiveness of minor defects in selectively tailoring and influencing these polarization processes, leading to high energy conversion efficiency in desired cross-coupling effects, such as EM coupling, the ECE, and dielectric properties.

Even after many decades of research and development of polymer ferroelectrics, there are still many unknowns regarding the polarization processes in polymer dielectrics and polymer ferroelectrics at the molecular scale, nanoscale, and mesoscale, which present great opportunities for future research and development considering the rich polymer chemistry in constructing

polymer molecules and nano- and mesoscale structures and the easy fabrication. Closely coupled experiments, theories, and characterization studies will lead to important insights into and uncover multiscale polarization processes and their cross-couplings to mechanical, thermal, magnetic, and optical effects. The hope is that these lead to enhanced performance, , such as ultrahigh coupling and a piezoelectric effect with no DC bias (Table 1), a giant ECE at much lower electric fields than that in Table 2, and tuning of the ferroelectric switching fields to any desired levels. Consequently, advances in the material performance will translate into the better performance for the various highlighted applications for example, wearable devices operated below the 50 V safe operation voltage defined by the Occupational Safety and Health Administration. Moreover, the potential exists for generating emerging applications with high performance, such as flexible and wearable magnetoelectric sensors for biomedical applications (*123*) or large-area flexible and robust multifunctional sensor arrays for hospital and nursing home beds.

In contrast to the widely available inorganic ferroelectrics that cover a wide range of applications, after more than 5 decades of research, PVDF-based ferroelectrics are still the lone polymer ferroelectric family that has been successfully used in many applications. Although ferroelectricity has been observed in odd-numbered nylons (in the 1980s) and many other polymers (*8, 9*), the low EM coupling and especially electroactive properties sensitive to environmental moisture prevent their practical use. Active polymer research exploiting the rich polarization processes and their underlying molecular structures, nanostructures and mesostructures for PVDF-based polymers has the potential to discover and develop next-generation classes of polymer ferroelectrics that are user-friendly, can be operated at much higher temperatures, and generate high electroactive couplings that rival those of PVDF-based polymers and even inorganic ferroelectrics.

Figures:

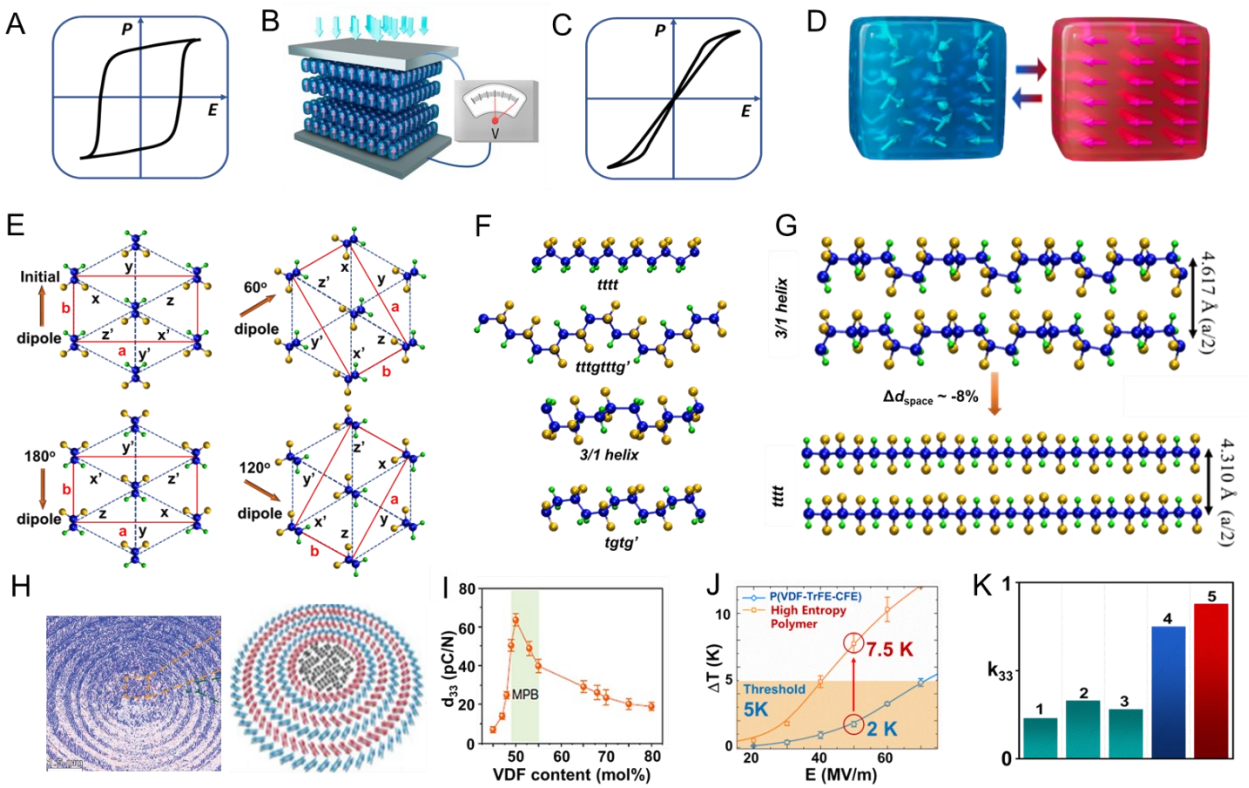

Fig. 1. **Underlying mechanism in polymer ferroelectrics** (A) Typical P-E loop of normal ferroelectric polymers. (B) Schematic of piezoelectricity. (C) Typical P-E loop of a relaxor ferroelectric polymer. (D) Schematics of electrothermal coupling. (E) Schematics of dipole rotation in the pseudo-hexagonal crystal structure and unit cell (red line) of β-phase PVDF (*27*). (F) Basic conformations, different interchain and intrachain combinations of which form various phases in PVDF polymers; *t – trans*, and *g/g' – gauche.* (G) Schematic of the geometry changes in a conformational change from *3/1 helix* to *tttt* (*27*). In (E to G), yellow atom – fluorine, blue atom – carbon, and green atom – hydrogen (*27*). (H) Toroidal topological texture self-organized in a ferroelectric P(VDF-TrFE) polymer (*47*). (I) Enhanced piezoelectric effect at the MPB of P(VDF-TrFE) copolymers (*48*). (J, K) Giant enhancement of the ECE (J) and EM coupling efficiency (K) in C=C modulated tetrapolymers (*22, 27*), 1-5 in (K) refer to the k_{33} in the following ferroelectric materials: 1. P(VDF-TrFE), 2. P(VDF-TrFE) single crystal, 3. P(VDF-TrFE) at the MPB, 4. PZT, and 5. P(VDF-TrFE-CFE-FA) (*27*). [(E) to (G) and (K) are adapted with permission from (27). (H), (I), and (J) are adapted with permission from (47), (48) copyright (2018) Springer Nature, and (22) copyright (2021) Springer Nature, respectively.]

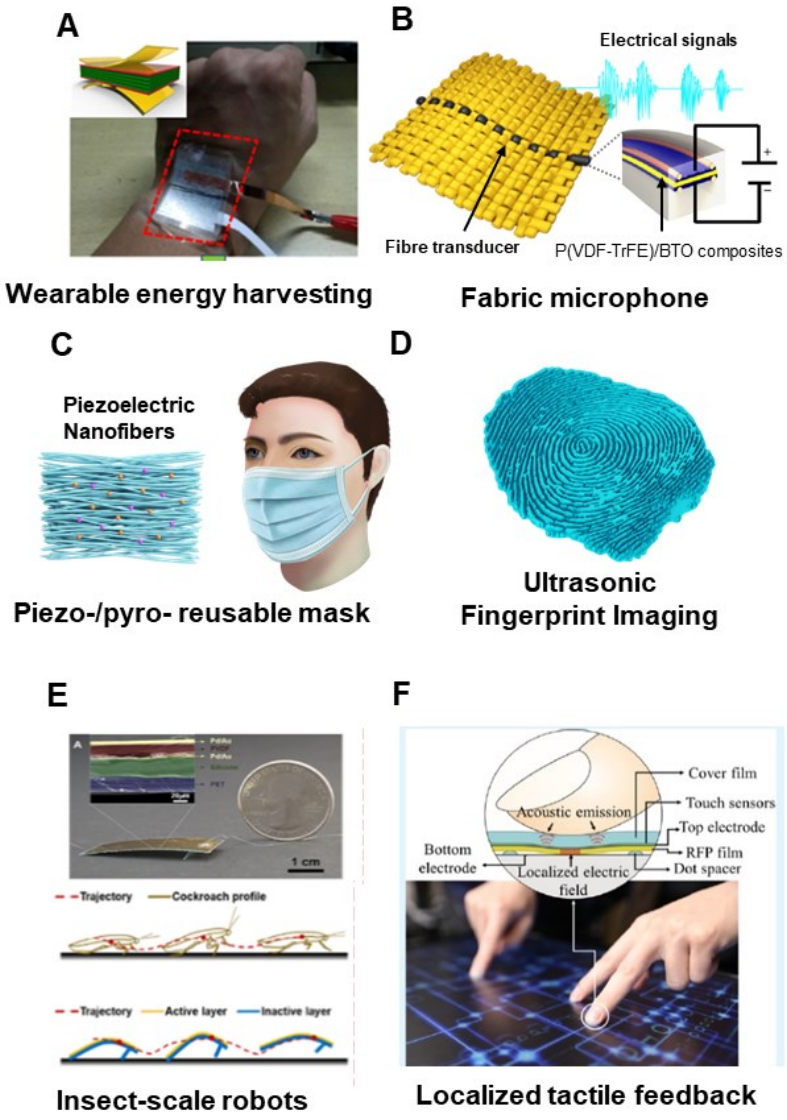

Fig. 2. **Advances in EM applications via PVDF-based polymers.** (A) Optical image of a wearable PVDF-based energy harvester. Schematic structure of a PENG and diagram of its flexibility. The inset shows a schematic of the device (red layer – aluminum foil, green layer – PVDF fibers, gold layer – PET) (*82*). (B) Schematic of PVDF/BTO composite fibers integrated with an acoustic fabric (*20*). (C) Schematic of a prototype piezoelectric polymer-based reusable mask (*26*). (D) Schematic of the finger pattern imagined by the Qualcomm finger scanner. (E) Upper panel: Optical photo showing an insect-scale robot. The inset scanning electron microscopy (SEM) image shows the cross-sectional view of the prototype robot with different layers of materials. Bottom panel: Comparison of the wavelike running paths showing the movement of the center of mass of a cockroach (*17*). (F) Schematic of PVDF relaxor-based localized tactile feedback devices (*25*). [(A), (B), (C), (D)/(E) and (F) adapted with permission from (*82*) copyright (2018) Elsevier, (*20*) copyright (2022) Springer Nature, (*26*) copyright (2022) Wiley, (*17*), and (*25*) copyright (2019) American Chemical Society, respectively.]

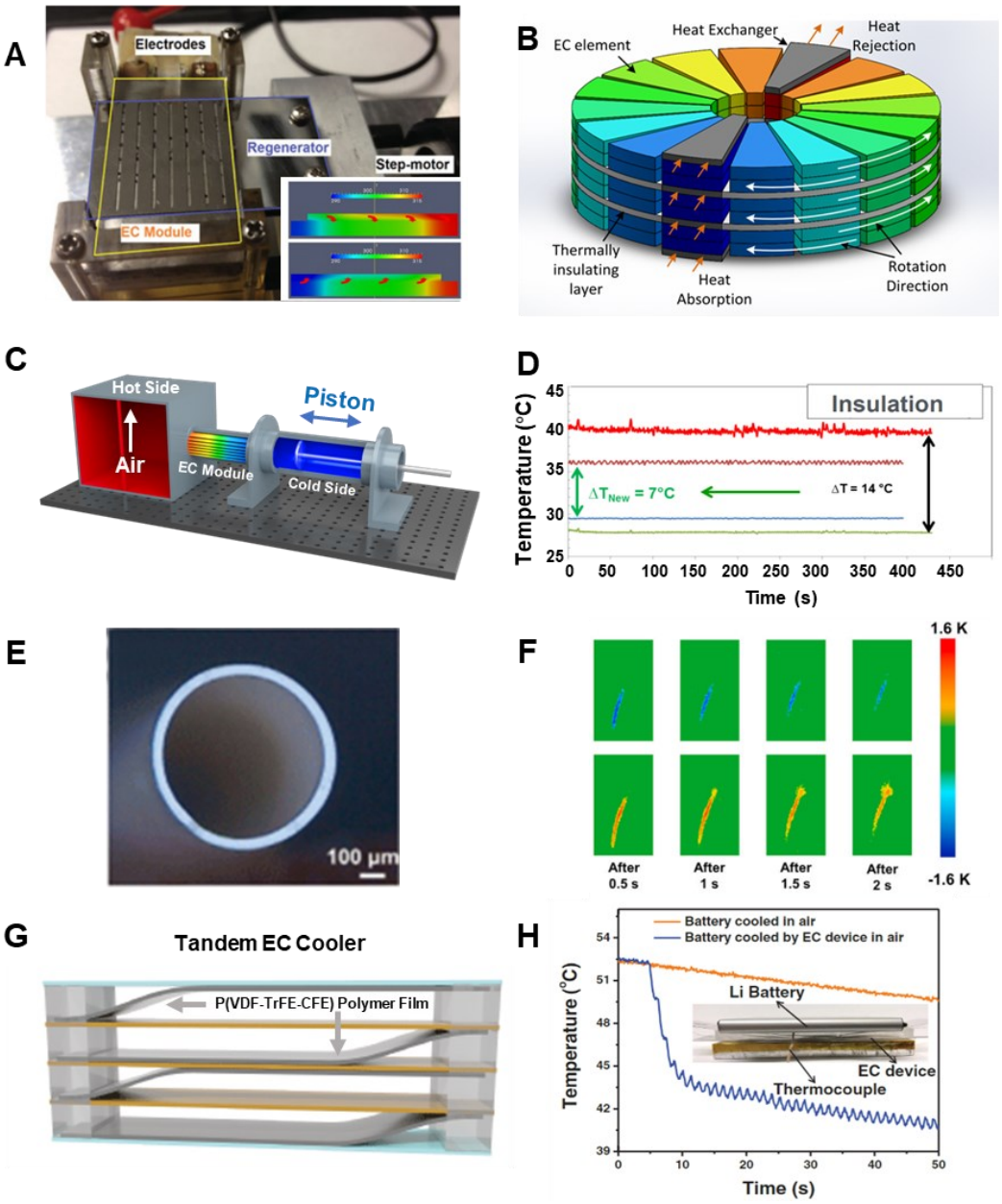

Fig. 3. **Advances in EC cooling technologies via PVDF-based polymers.** Prototypes of EC refrigerators operating ferroelectric polymers as solid-state refrigerants. (A) All-solid EC cooling device utilizing e-beam irradiated copolymers and operating under an AER cycle (*56*). (B) Schematic of an ML rotary EC cooling device operating under an AER cycle. (C, D) Schematics of the EC refrigerator utilizing a fluid (air) as the regenerator (C); a maximum temperature span of 14 K was achieved (*91*). (E, F) Cooling tube made of relaxor ferroelectric polymers (E) providing heating and cooling to the fluids that pass through it (F) (*94*). (G, H) Tandem EC prototype utilizing electrostatic oscillation (G) to operate the refrigeration cycle and introduce rapid cooling to a lithium battery (H) (*23, 24*). [(A) to (H) adapted with permission from (*56*) AIP Publishing, (*91*), (*94*) copyright (2022) Elsevier, (*23*) and (*24*) copyright (2022) Springer Nature.]

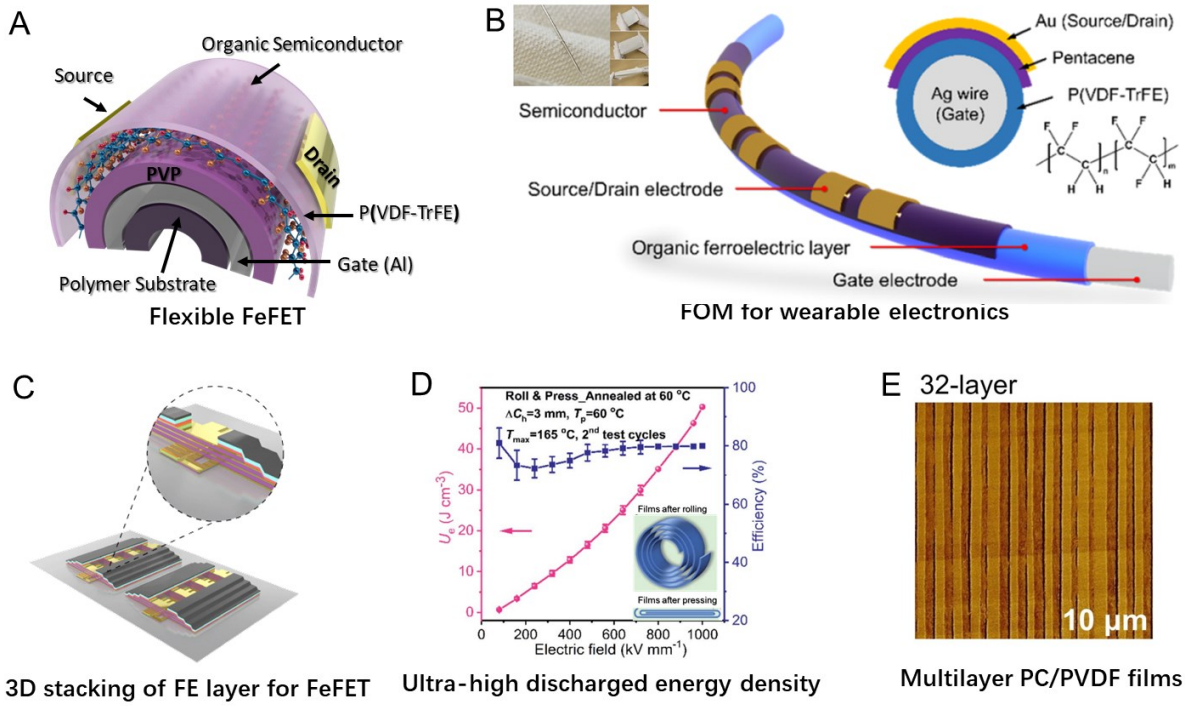

Fig. 4. **Advanced dielectric applications for PVDF-based polymers.** (A) Schematic of highly bent FeFET memory with P(VDF-TrFE) as the gate dielectric (*98*). (B) Schematic of fiber organic memory (FOM) based on P(VDF-TrFE). The insert presents a fabric with the FOM integrated (*103*). (C) Schematic of 3D stacking of the ferroelectric layer, *i.e.*, P(VDF-TrFE), in a FeFET device (*106*). (D) Discharged energy density for PVDF films after continuous folding. The insert indicates that the film was prepared by rolling and pressing (*115*). (E) Atomic force microscopy (AFM) image of PC/PVDF ML films, *i.e.,* 32 layers with a thickness of 400 nm for each layer (*116*). [(A), (B), (C), (D) and (E) adapted with permission from (*98*), (*103*) copyright (2019) American Chemical Society, (*106*) copyright (2019) Elsevier, (*115*) and (*116*) copyright (2017) Elsevier, respectively.]

Table 1: **Advances in the EM performance.** Summary of piezoelectric effects and EM couplings for PVDF-based polymers and comparison with ceramic PZT (*2, 9, 27*)

Material	**DC bias (MV/m)**	d_{33} **(pm/V)**	k_{33}	K $(\varepsilon/\varepsilon_0)$	g_{33} **(Vm/N)**	Y **(GPa)**	**Acoustic impedance ($Gg/(m^2s)$)**
PVDF	0	-31.5	0.11	11	- 0.32	3	3
P(VDF-TrFE)	0	-33.5	0.3	8	- 0.47	3.3	4
PZT Piezoceramic	0	650	0.75	3,800	0.019	50	33.7
P(VDF-TrFE-CFE-FA) 63/29.7/5.4/1.9	40	-858	0.74	34	-2.85	0.22	/
P(VDF-TrFE-CFE-FA) s-63/29.7/5.4/1.9	40	-1050	0.88	36	-3.29	0.22	/
P(VDF-TrFE-CFE-FA) 63.6/30/4.4/2	20	-1177	0.71	64	-2.08	0.21	/

*s-63/29.7/5.4/1.9 is a uniaxially stretched film

Table 2: Advances in the EC effect. Summary of the EC performance for PVDF-based polymers and their inorganic nanocomposites.

Material	T (K)	ΔE (MV/m)	ΔS (J/kgK)	ΔT (K)	Ref.
Terpolymer P(VDF-TrFE-CFE) 59.2/33.6/7.2 mol%	303	150	80	16	(*39*)
Irradiated P(VDF-TrFE)	323	50/180	28/160	6.2/35	(*51*)
P(VDF-TrFE-CFE)/BNNSs/BST1/2/3	273~333	200	170	35	(*58*)
P(VDF-TrFE-CFE)/BST_nfs	303	200	105	44.3	(*59*)
P(VDF-TrFE-CFE)/BST_nfs	300	70	49	11.3	(*124*)
P(VDF-TrFE-CFE)/BFBZT	303	75	78	13.8	(*19*)
P(VDF-TrFE-CFE)-Ceramic Scaffold	300	60	26.8	6	(*125*)
PBZ-nfs/PVDF	243	150	52.7	14	(*126*)
P(VDF-TrFE-CFE)/BTO	308	125	2.6	/	*(127)*
P(VDF-TrFE-CFE-DB)-BST-15	RT	100	6.5	/	(*128*)
P(VDF-TrFE-CTFE-FA)	313	80	12.5	2.5	(*65*)
P(VDF-TrFE-CFE-FA)	303	50/80	38/70	7.5/14	(*22*)

References and Notes

1. M. E. Lines, A. M. Glass, *Principles and applications of ferroelectrics and related materials*. (Oxford University Press, 2001).
2. K. Uchino, *Ferroelectric devices*. (CRC press, 2018).
3. H. Kawai, The Piezoelectricity of Poly (vinylidene Fluoride). *Japanese Journal of Applied Physics* **8**, 975 (1969).
4. G. T. Davis, J. E. McKinney, M. G. Broadhurst, S. C. Roth, Electric-field-induced phase changes in poly(vinylidene fluoride). *Journal of Applied Physics* **49**, 4998-5002 (1978).
5. R. G. Kepler, R. A. Anderson, Ferroelectricity in polyvinylidene fluoride. *Journal of Applied Physics* **49**, 1232-1235 (1978).
6. T. Furukawa, M. Date, E. Fukada, Y. Tajitsu, A. Chiba, Ferroelectric behavior in the copolymer of vinylidenefluoride and trifluoroethylene. *Japanese Journal of Applied Physics* **19**, L109-L112 (1980).
7. T. Yagi, M. Tatemoto, J.-i. Sako, Transition behavior and dielectric properties in trifluoroethylene and vinylidene fluoride copolymers. *Polymer Journal* **12**, 209-223 (1980).
8. A. J. Lovinger, Ferroelectric polymers. *Science* **220**, 1115 (1983).
9. *Ferroelectric polymers: chemistry: physics, and applications*. H. S. Nalwa Ed., (Marcel Dekker, New York 1995).
10. L. E. Cross, Relaxor ferroelectrics. *Ferroelectrics* **76**, 241-267 (1987).
11. Q. M. Zhang, V. Bharti, X. Zhao, Giant electrostrictive response and ferroelectric relaxor behavior in electron irradiated P (VDF-TrFE) Polymer. *Science* **280**, 2101-2104 (1998).
12. F. Xia, Z. Y. Cheng, H. S. Xu, H. F. Li, Q. M. Zhang, G. J. Kavarnos, R. Y. Ting, G. Abdul-Sadek, K. Belfield, High electromechanical responses in a poly(vinylidene fluoride–trifluoroethylene–chlorofluoroethylene) terpolymer. *Advanced Materials* **14**, 1574-1577 (2002).
13. R. Newnham, V. Sundar, R. Yimnirun, J. Su, Q. Zhang, Electrostriction: nonlinear electromechanical coupling in solid dielectrics. *The Journal of Physical Chemistry B* **101**, 10141-10150 (1997).
14. B. Neese, B. Chu, S.-G. Lu, Y. Wang, E. Furman, Q. M. Zhang, Large electrocaloric effect in ferroelectric polymers near room temperature. *Science* **321**, 821-823 (2008).
15. X. Li, S.-G. Lu, X.-Z. Chen, H. Gu, X.-s. Qian, Q. M. Zhang, Pyroelectric and electrocaloric materials. *Journal of Materials Chemistry C* **1**, 23-37 (2013).
16. F. S. Foster, K. A. Harasiewicz, M. D. Sherar, A history of medical and biological imaging with polyvinylidene fluoride (PVDF) transducers. *IEEE Transactions on Ultrasonics, Ferroelectrics, and Frequency Control* **47**, 1363-1371 (2000).
17. Y. Wu, J. K. Yim, J. Liang, Z. Shao, M. Qi, J. Zhong, Z. Luo, X. Yan, M. Zhang, X. Wang, Insect-scale fast moving and ultrarobust soft robot. *Science Robotics* **4**, eaax1594 (2019).
18. W. Yang, W. Gong, C. Hou, Y. Su, Y. Guo, W. Zhang, Y. Li, Q. Zhang, H. Wang, All-fiber tribo-ferroelectric synergistic electronics with high thermal-moisture stability and comfortability. *Nature Communications* **10**, 5541 (2019).
19. Y. Chen, J. Qian, J. Yu, M. Guo, Q. Zhang, J. Jiang, Z. Shen, L.-Q. Chen, Y. Shen, An all-scale hierarchical architecture induces colossal room-temperature electrocaloric effect at ultralow electric field in polymer nanocomposites. *Advanced Materials* **32**, 1907927 (2020).
20. W. Yan, G. Noel, G. Loke, E. Meiklejohn, T. Khudiyev, J. Marion, G. Rui, J. Lin, J. Cherston, A. Sahasrabudhe, Single fibre enables acoustic fabrics via nanometre-scale vibrations. *Nature* **603**, 616-623 (2022).
21. S. Zhang, Regenerative face mask with long shelf life and long service time for effective coronavirus filtration. *SBIR Phase I (CDC)*, (2022).

22. X. Qian, D. Han, L. Zheng, J. Chen, M. Tyagi, Q. Li, F. Du, S. Zheng, X. Huang, S. Zhang, J. Shi, H. Huang, X. Shi, J. Chen, H. Qin, J. Bernholc, X. Chen, L.-Q. Chen, L. Hong, Q. M. Zhang, High-entropy polymer produces a giant electrocaloric effect at low fields. *Nature* **600**, 664-669 (2021).
23. R. Ma, Z. Zhang, K. Tong, D. Huber, R. Kornbluh, Y. S. Ju, Q. Pei, Highly efficient electrocaloric cooling with electrostatic actuation. *Science* **357**, 1130-1134 (2017).
24. Y. Meng, Z. Zhang, H. Wu, R. Wu, J. Wu, H. Wang, Q. Pei, A cascade electrocaloric cooling device for large temperature lift. *Nature Energy* **5**, 996-1002 (2020).
25. Q. V. Duong, V. P. Nguyen, F. Domingues Dos Santos, S. T. Choi, Localized fretting-vibrotactile sensations for large-area displays. *ACS Applied Materials and Interfaces* **11**, 33292-33301 (2019).
26. T. T. Le, E. J. Curry, T. Vinikoor, R. Das, Y. Liu, D. Sheets, K. T. Tran, C. J. Hawxhurst, J. F. Stevens, J. N. Hancock, Piezoelectric nanofiber membrane for reusable, stable, and highly functional face mask filter with long‐term biodegradability. *Advanced Functional Materials* **32**, 2113040 (2022).
27. X. Chen, H. Qin, X. Qian, W. Zhu, B. Li, B. Zhang, W. Lu, R. Li, S. Zhang, L. Zhu, F. domingues dos santos, J. Bernholc, Q. M. Zhang, Relaxor ferroelectric polymer exhibits ultrahigh electromechanical coupling at low electric field. *Science* **375**, 1418-1422 (2022).
28. C. Z. Rosen, B. V. Hiremath, R. Newnham, in *Proc. Piezoelectricity, Amer. Inst. Physi.* (1992), pp. 227-228.
29. Z. Y. Cheng, Q. M. Zhang, Field-activated electroactive polymers. *MRS Bulletin* **33**, 183-187 (2008).
30. G. J. Velders, D. W. Fahey, J. S. Daniel, M. McFarland, S. O. Andersen, The large contribution of projected HFC emissions to future climate forcing. *Proceedings of the National Academy of Sciences of the United States of America* **106**, 10949-10954 (2009).
31. P. Hawken, *Drawdown: The most comprehensive plan ever proposed to reverse global warming*. (Penguin, 2017).
32. J. Shi, D. Han, Z. Li, L. Yang, S.-G. Lu, Z. Zhong, J. Chen, Q. Zhang, X. Qian, Electrocaloric cooling materials and devices for zero-global-warming-potential, high-efficiency refrigeration. *Joule* **3**, 1200-1225 (2019).
33. P. Kobeco, I. Kurtchatov, Dielectric properties of Rochelle salt crystal. *Zeitschrift für Physik* **66**, 192-205 (1930).
34. G. G. Wiseman, J. K. Kuebler, Electrocaloric effect in ferroelectric Rochelle salt. *Physical Review* **131**, 2023-2027 (1963).
35. Y. V. Sinyavsky, N. Pashkov, Y. Gorovoy, G. Lugansky, L. Shebanov, The optical ferroelectric ceramic as working body for electrocaloric refrigeration. *Ferroelectrics* **90**, 213-217 (1989).
36. Y. V. Sinyavsky, V. M. Brodyansky, Experimental testing of electrocaloric cooling with transparent ferroelectric ceramic as a working body. *Ferroelectrics* **131**, 321-325 (1992).
37. X. Moya, S. Kar-Narayan, N. D. Mathur, Caloric materials near ferroic phase transitions. *Nature Materials* **13**, 439-450 (2014).
38. S.-G. Lu, B. Rožič, Q. M. Zhang, Z. Kutnjak, X. Li, E. Furman, L. Gorny, M. Lin, B. Malic, M. Kosec, R. Blinc, R. Pirc, Organic and inorganic relaxor ferroelectrics with giant electrocaloric effect. *Applied Physics Letters* **97**, 162904 (2010).
39. X. Li, X.-s. Qian, S. Lu, J. Cheng, Z. Fang, Q. M. Zhang, Tunable temperature dependence of electrocaloric effect in ferroelectric relaxor poly (vinylidene fluoride-trifluoroethylene-chlorofluoroethylene terpolymer. *Applied Physics Letters* **99**, 052907 (2011).
40. F. Xu, S. Trolier-McKinstry, W. Ren, B. Xu, Z.-L. Xie, K. Hemker, Domain wall motion and its contribution to the dielectric and piezoelectric properties of lead zirconate titanate films. *Journal of Applied Physics* **89**, 1336-1348 (2001).
41. X. Chen, H. Qin, W. Zhu, B. Zhang, W. Lu, J. Bernholc, Q. Zhang, Giant electrostriction enabled by defect-induced critical phenomena in relaxor ferroelectric polymers. *Macromolecules*, (2023).

42. S. Anwar, D. Pinkal, W. Zajaczkowski, P. Von Tiedemann, H. Sharifi Dehsari, M. Kumar, T. Lenz, U. Kemmer-Jonas, W. Pisula, M. Wagner, Solution-processed transparent ferroelectric nylon thin films. *Science Advances* **5**, eaav3489 (2019).
43. Q. Li, Q. Wang, Ferroelectric polymers and their energy‐related applications. *Macromolecular Chemistry and Physics* **217**, 1228-1244 (2016).
44. A. J. Lovinger, D. D. Davis, R. E. Cais, J. M. Kometani, The role of molecular defects on the structure and phase transitions of poly (vinylidene fluoride). *Polymer* **28**, 617-626 (1987).
45. G. Rui, Y. Huang, X. Chen, R. Li, D. Wang, T. Miyoshi, L. Zhu, Giant spontaneous polarization for enhanced ferroelectric properties of biaxially oriented poly (vinylidene fluoride) by mobile oriented amorphous fractions. *Journal of Materials Chemistry C* **9**, 894-907 (2021).
46. A. V. Bune, V. M. Fridkin, S. Ducharme, L. M. Blinov, S. P. Palto, A. V. Sorokin, S. Yudin, A. Zlatkin, Two-dimensional ferroelectric films. *Nature* **391**, 874-877 (1998).
47. M. Guo, C. Guo, J. Han, S. Chen, S. He, T. Tang, Q. Li, J. Strzalka, J. Ma, D. Yi, K. Wang, B. Xu, P. Gao, H. Huang, L.-Q. Chen, S. Zhang, Y.-H. Lin, C.-W. Nan, Y. Shen, Toroidal polar topology in strained ferroelectric polymer. *Science* **371**, 1050-1056 (2021).
48. Y. Liu, H. Aziguli, B. Zhang, W. Xu, W. Lu, J. Bernholc, Q. Wang, Ferroelectric polymers exhibiting behaviour reminiscent of a morphotropic phase boundary. *Nature* **562**, 96-100 (2018).
49. V. S. Bystrov, E. V. Paramonova, I. K. Bdikin, A. V. Bystrova, R. C. Pullar, A. L. Kholkin, Molecular modeling of the piezoelectric effect in the ferroelectric polymer poly (vinylidene fluoride)(PVDF). *Journal of molecular modeling* **19**, 3591-3602 (2013).
50. S. G. Lu, Q. M. Zhang, Electrocaloric materials for solid‐state refrigeration. *Advanced Materials* **21**, 1983-1987 (2009).
51. X. Li, X.-S. Qian, H. Gu, X. Chen, S. G. Lu, M. Lin, F. Bateman, Q. M. Zhang, Giant electrocaloric effect in ferroelectric poly(vinylidenefluoride-trifluoroethylene) copolymers near a first-order ferroelectric transition. *Applied Physics Letters* **101**, 132903 (2012).
52. T. C. Chung, A. Petchsuk, Synthesis and properties of ferroelectric fluoroterpolymers with Curie transition at ambient temperature. *Macromolecules* **35**, 7678-7684 (2002).
53. H. Xu, Z.-Y. Cheng, D. Olson, T. Mai, Q. M. Zhang, G. Kavarnos, Ferroelectric and electromechanical properties of poly (vinylidene-fluoride–trifluoroethylene–chlorotrifluoroethylene) terpolymer. *Applied Physics Letters* **78**, 2360-2362 (2001).
54. J. Shi, Q. Li, T. Gao, D. Han, Y. Li, J. Chen, X. Qian, Numerical evaluation of a kilowatt-level rotary electrocaloric refrigeration system. *International Journal of Refrigeration* **121**, 279-288 (2021).
55. X. Moya, N. Mathur, Caloric materials for cooling and heating. *Science* **370**, 797-803 (2020).
56. H. Gu, X. Qian, X. Li, B. Craven, W. Zhu, A. Cheng, S. C. Yao, Q. M. Zhang, A chip scale electrocaloric effect based cooling device. *Applied Physics Letters* **102**, 122904 (2013).
57. J. Qian, J. Jiang, Y. Shen, Enhanced electrocaloric strength in P (VDF-TrFE-CFE) by decreasing the crystalline size. *Journal of Materiomics* **5**, 357-362 (2019).
58. G. Zhang, B. Fan, P. Zhao, Z. Hu, Y. Liu, F. Liu, S. Jiang, S. Zhang, H. Li, Q. Wang, Ferroelectric polymer nanocomposites with complementary nanostructured fillers for electrocaloric cooling with high power density and great efficiency. *ACS Applied Energy Materials* **1**, 1344-1354 (2018).
59. J. Qian, R. Peng, Z. Shen, J. Jiang, F. Xue, T. Yang, L. Chen, Y. Shen, Interfacial coupling boosts giant electrocaloric effects in relaxor polymer nanocomposites: in situ characterization and phase‐field simulation. *Advanced Materials* **31**, 1801949 (2019).
60. Y. Liu, B. Zhang, W. Xu, H. Aziguli, Z. Han, W. Lu, J. Bernholc, Q. Wang, Chirality-induced relaxor properties in ferroelectric polymers. *Nature Materials* **19**, 1169-1174 (2020).

61. S. Qian, D. Nasuta, A. Rhoads, Y. Wang, Y. Geng, Y. Hwang, R. Radermacher, I. Takeuchi, Not-in-kind cooling technologies: A quantitative comparison of refrigerants and system performance. *International Journal of Refrigeration* **62**, 177-192 (2015).
62. A. Torelló, P. Lheritier, T. Usui, Y. Nouchokgwe, M. Gérard, O. Bouton, S. Hirose, E. Defay, Giant temperature span in electrocaloric regenerator. *Science* **370**, 125-129 (2020).
63. B. Nair, T. Usui, S. Crossley, S. Kurdi, G. Guzmán-Verri, X. Moya, S. Hirose, N. Mathur, Large electrocaloric effects in oxide multilayer capacitors over a wide temperature range. *Nature* **575**, 468-472 (2019).
64. D. H. Kim, H. S. Park, M. S. Kim, The effect of the refrigerant charge amount on single and cascade cycle heat pump systems. *International journal of refrigeration* **40**, 254-268 (2014).
65. F. Le Goupil, K. Kallitsis, S. Tencé-Girault, N. Pouriamanesh, C. Brochon, E. Cloutet, T. Soulestin, F. Domingue Dos Santos, N. Stingelin, G. Hadziioannou, Enhanced electrocaloric response of vinylidene fluoride–based polymers via one-step molecular engineering. *Advanced Functional Materials* **31**, 2007043 (2021).
66. S. T. Choi, J. O. Kwon, F. Bauer, Multilayered relaxor ferroelectric polymer actuators for low-voltage operation fabricated with an adhesion-mediated film transfer technique. *Sensors and Actuators A: Physical* **203**, 282-290 (2013).
67. E. Häsler, L. Stein, G. Harbauer, Implantable physiological power supply with PVDF film. *Ferroelectrics* **60**, 277-282 (1984).
68. J. Kymissis, C. Kendall, J. Paradiso, N. Gershenfeld, in *Digest of Papers. Second International Symposium on Wearable Computers (Cat. No. 98EX215)*. (IEEE, 1998), pp. 132-139.
69. A. Ranjan, C. Peng, S. Wagle, F. Melandsø, A. Habib, High-frequency acoustic imaging using adhesive-free polymer transducer. *Polymers* **13**, 1462 (2021).
70. C. Yang, S. Song, F. Chen, N. Chen, Fabrication of PVDF/BaTiO3/CNT piezoelectric energy harvesters with bionic balsa wood structures through 3D printing and supercritical carbon dioxide foaming. *ACS Applied Materials & Interfaces* **13**, 41723-41734 (2021).
71. S. Panda, S. Hajra, H. Jeong, B. K. Panigrahi, P. Pakawanit, D. Dubal, S. Hong, H. J. Kim, Biocompatible CaTiO3-PVDF composite-based piezoelectric nanogenerator for exercise evaluation and energy harvesting. *Nano Energy* **102**, 107682 (2022).
72. Y. Wang, T. Guo, Z. Tian, K. Bibi, Y. Z. Zhang, H. N. Alshareef, MXenes for energy harvesting. *Advanced Materials* **34**, 2108560 (2022).
73. F. Jiang, X. Zhou, J. Lv, J. Chen, J. Chen, H. Kongcharoen, Y. Zhang, P. S. Lee, Stretchable, breathable, and stable lead‐free perovskite/polymer nanofiber composite for Hybrid Triboelectric and Piezoelectric Energy Harvesting. *Advanced Materials* **34**, 2200042 (2022).
74. H. Hatcher, Energy-harvesting clothes. *Nature Reviews Materials* **7**, 256 (2022).
75. N. Sezer, M. Koç, A comprehensive review on the state-of-the-art of piezoelectric energy harvesting. *Nano Energy* **80**, 105567 (2021).
76. J. Fu, Y. Hou, X. Gao, M. Zheng, M. Zhu, Highly durable piezoelectric energy harvester based on a PVDF flexible nanocomposite filled with oriented BaTi2O5 nanorods with high power density. *Nano Energy* **52**, 391-401 (2018).
77. Y. M. Yousry, K. Yao, A. M. Mohamed, W. H. Liew, S. Chen, S. Ramakrishna, Theoretical model and outstanding performance from constructive piezoelectric and triboelectric mechanism in electrospun PVDF fiber film. *Advanced Functional Materials* **30**, 1910592 (2020).
78. F. Mokhtari, G. M. Spinks, C. Fay, Z. Cheng, R. Raad, J. Xi, J. Foroughi, Wearable electronic textiles from nanostructured piezoelectric fibers. *Advanced Materials Technologies* **5**, 1900900 (2020).
79. H. Gao, P. T. Minh, H. Wang, S. Minko, J. Locklin, T. Nguyen, S. Sharma, High-performance flexible yarn for wearable piezoelectric nanogenerators. *Smart Materials and Structures* **27**, 095018 (2018).

80. K. Castkova, J. Kastyl, D. Sobola, J. Petrus, E. Stastna, D. Riha, P. Tofel, Structure–properties relationship of electrospun pvdf fibers. *Nanomaterials* **10**, 1221 (2020).
81. L. Persano, C. Dagdeviren, Y. Su, Y. Zhang, S. Girardo, D. Pisignano, Y. Huang, J. A. Rogers, High performance piezoelectric devices based on aligned arrays of nanofibers of poly (vinylidenefluoride-co-trifluoroethylene). *Nature Communications* **4**, 1633 (2013).
82. K. Shi, B. Sun, X. Huang, P. Jiang, Synergistic effect of graphene nanosheet and BaTiO3 nanoparticles on performance enhancement of electrospun PVDF nanofiber mat for flexible piezoelectric nanogenerators. *Nano Energy* **52**, 153-162 (2018).
83. C. Peng, M. Chen, H. Wang, J. Shen, X. Jiang, P (VDF-TrFE) thin-film-based transducer for under-display ultrasonic fingerprint sensing applications. *IEEE Sensors Journal* **20**, 11221-11228 (2020).
84. S. Biswas, Y. Visell, Haptic perception, mechanics, and material technologies for virtual reality. *Advanced Functional Materials* **31**, 2008186 (2021).
85. W. Bruno, S. Merighi, V. Parkula, F. Jeanneau, The Science of Touch in Electronics Haptics, it used to be all about resonant frequency. 2021.
86. H. Gu, X.-S. Qian, H.-J. Ye, Q. M. Zhang, An electrocaloric refrigerator without external regenerator. *Applied Physics Letters* **105**, 162905 (2014).
87. H. Gu, B. Craven, X. Qian, X. Li, A. Cheng, Q. M. Zhang, Simulation of chip-size electrocaloric refrigerator with high cooling-power density. *Applied Physics Letters* **102**, 112901 (2013).
88. Y. Wang, Z. Zhang, T. Usui, M. Benedict, S. Hirose, J. Lee, J. Kalb, D. Schwartz, A high-performance solid-state electrocaloric cooling system. *Science* **370**, 129-133 (2020).
89. T. Zhang, X.-S. Qian, H. Gu, Y. Hou, Q. Zhang, An electrocaloric refrigerator with direct solid to solid regeneration. *Applied Physics Letters* **110**, 243503 (2017).
90. H. Hou, S. Qian, I. Takeuchi, Materials, physics and systems for multicaloric cooling. *Nature Reviews Materials* **7**, 633-652 (2022).
91. S. Ravi Annapragada, P. Verma, A. Sur, W. Xie. (UTRC, 2017 Building Technologies Office Peer Review, 2017). https://www.energy.gov/sites/default/files/2017/04/f34/7_312111_Annapragada_031517-1430.pdf
92. D. Guo, J. Gao, Y.-J. Yu, S. Santhanam, A. Slippey, G. K. Fedder, A. J. McGaughey, S.-C. Yao, Design and modeling of a fluid-based micro-scale electrocaloric refrigeration system. *International Journal of Heat and Mass Transfer* **72**, 559-564 (2014).
93. U. Plaznik, A. Kitanovski, B. Rožič, B. Malič, H. Uršič, S. Drnovšek, J. Cilenšek, M. Vrabelj, A. Poredoš, Z. Kutnjak, Bulk relaxor ferroelectric ceramics as a working body for an electrocaloric cooling device. *Applied Physics Letters* **106**, 043903 (2015).
94. H. Cui, Q. Zhang, Y. Bo, P. Bai, M. Wang, C. Zhang, X. Qian, R. Ma, Flexible microfluidic electrocaloric cooling capillary tube with giant specific device cooling power density. *Joule* **6**, 258-268 (2022).
95. Y. Bo, Q. Zhang, H. Cui, M. Wang, C. Zhang, W. He, X. Fan, Y. Lv, X. Fu, J. Liang, Electrostatic actuating double‐unit electrocaloric cooling device with high efficiency. *Advanced Energy Materials* **11**, 2003771 (2021).
96. W. Ji, B. Cao, Y. Geng, Y. Zhu, B. Lin, Study on human skin temperature and thermal evaluation in step change conditions: From non-neutrality to neutrality. *Energy and Buildings* **156**, 29-39 (2017).
97. K. L. Kim, W. Lee, S. K. Hwang, S. H. Joo, S. M. Cho, G. Song, S. H. Cho, B. Jeong, I. Hwang, J.-H. Ahn, Epitaxial growth of thin ferroelectric polymer films on graphene layer for fully transparent and flexible nonvolatile memory. *Nano Letters* **16**, 334-340 (2016).
98. R. H. Kim, H. J. Kim, I. Bae, S. K. Hwang, D. B. Velusamy, S. M. Cho, K. Takaishi, T. Muto, D. Hashizume, M. Uchiyama, Non-volatile organic memory with sub-millimetre bending radius. *Nature Communications* **5**, 3583 (2014).

99. M. Xu, X. Zhang, S. Li, T. Xu, W. Xie, W. Wang, Gate-controlled multi-bit nonvolatile ferroelectric organic transistor memory on paper substrates. *Journal of Materials Chemistry C* **7**, 13477-13485 (2019).
100. R. C. G. Naber, C. Tanase, P. W. M. Blom, G. H. Gelinck, A. W. Marsman, F. J. Touwslager, S. Setayesh, D. M. de Leeuw, High-performance solution-processed polymer ferroelectric field-effect transistors. *Nature Materials* **4**, 243-248 (2005).
101. B. Tian, J. Wang, S. Fusil, Y. Liu, X. Zhao, S. Sun, H. Shen, T. Lin, J. Sun, C. Duan, Tunnel electroresistance through organic ferroelectrics. *Nature Communications* **7**, 1502 (2016).
102. H. Li, R. Wang, S.-T. Han, Y. Zhou, Ferroelectric polymers for non-volatile memory devices: a review. *Polymer International* **69**, 533-544 (2020).
103. M. Kang, S. Lee, S. Jang, S. Hwang, S.-K. Lee, S. Bae, J.-M. Hong, S. H. Lee, K.-U. Jeong, J. Lim, T.-W. Kim, Low-voltage organic transistor memory fiber with a nanograined organic ferroelectric film. *ACS Applied Materials and Interfaces* **11**, 22575-22582 (2019).
104. Y. Chen, M. Xu, X. Hu, Y. Yue, X. zhang, Q.-D. Shen, High resolution structural mapping and single-domain switching kinetics in the 2D-confined ferroelectric nanodots for low-power FeRAM. *Nanoscale* **12**, 11997-12006 (2020).
105. Z. Hu, M. Tian, B. Nysten, A. Jonas, Regular arrays of highly ordered ferroelectric polymer nanostructures for non-volatile low-voltage memories. *Nature Materials* **8**, 62-67 (2009).
106. S. Hwang, K. Kim, S. Cho, T. Park, B. Jeong, I. Bae, C. Park, Multi-level operation of three-dimensionally stacked non-volatile ferroelectric polymer memory with high-performance hole-injection layer. *Organic Electronics* **75**, 105394 (2019).
107. S. K. Hwang, S. M. Cho, K. L. Kim, C. Park, 3D‐Stacked vertical channel nonvolatile polymer memory. *Advanced Electronic Materials* **1**, 1400042 (2015).
108. M. Carroli, A. Dixon, M. Herder, E. Pavlica, S. Hecht, G. Bratina, E. Orgiu, P. Samorì, Multiresponsive nonvolatile memories based on optically switchable ferroelectric organic field-effect transistors. *Advanced Materials* **33**, 2007965 (2021).
109. S. He, M. Guo, W. Yue, L. Yuhan, Y. Shen, An optical/ferroelectric multiplexing multidimensional non‐volatile memory from ferroelectric polymer. *Advanced Materials* **34**, 2202181 (2022).
110. Z. Yin, B. Tian, Q. Zhu, C. Duan, Characterization and application of PVDF and its copolymer Films prepared by spin-coating and langmuir–blodgett method. *Polymers* **11**, 2033 (2019).
111. S. Majumdar, B. Chen, Q. Qin, H. Majumdar, S. Dijken, Electrode dependence of tunneling electroresistance and switching stability in organic ferroelectric P(VDF-TrFE)-based tunnel junctions. *Advanced Functional Materials* **28**, 1703273 (2018).
112. B. Chu, X. Zhou, K. Ren, B. Neese, M. Lin, Q. Wang, F. Bauer, Q. Zhang, A dielectric polymer with high electric energy density and fast discharge speed. *Science* **313**, 334-336 (2006).
113. N. Meng, X. Ren, G. Santagiuliana, L. Ventura, H. Zhang, J. Wu, H. Yan, M. Reece, E. Bilotti, Ultrahigh β-phase content poly(vinylidene fluoride) with relaxor-like ferroelectricity for high energy density capacitors. *Nature Communications* **10**, 4535 (2019).
114. J. P. DiMarco, Implantable cardioverter–defibrillators. *New England Journal of Medicine* **349**, 1836-1847 (2003).
115. X. Ren, N. Meng, L. Ventura, S. Goutianos, E. Barbieri, H. Zhang, H. Yan, M. J. Reece, E. Bilotti, Ultra-high energy density integrated polymer dielectric capacitors. *Journal of Materials Chemistry A* **10**, 10171-10180 (2022).
116. E. Baer, L. Zhu, 50th anniversary perspective: dielectric phenomena in polymers and multilayered dielectric films. *Macromolecules* **50**, 2239-2256 (2017).
117. T. Ju, X. Chen, D. Langhe, M. Ponting, E. Baer, L. Zhu, Enhancing breakdown strength and lifetime of multilayer dielectric films by using high temperature polycarbonate skin layers. *Energy Storage Materials* **45**, 494-503 (2022).

118. H. Li, T. Yang, Y. Zhou, D. Ai, B. Yao, Y. Liu, L. Li, L.-Q. Chen, Q. Wang, Enabling high-energy-density high-efficiency ferroelectric polymer nanocomposites with rationally designed nanofillers. *Advanced Functional Materials* **31**, 2006739 (2021).
119. G. Zhang, Q. Li, E. Allahyarov, Y. Li, L. Zhu, Challenges and opportunities of polymer nanodielectrics for capacitive energy storage. *ACS Applied Materials & Interfaces* **13**, 37939-37960 (2021).
120. Y. Thakur, T. Zhang, C. Iacob, T. Yang, J. Bernholc, L. Chen, J. Runt, Q. M. Zhang, Enhancement of the dielectric response in polymer nanocomposites with low dielectric constant fillers. *Nanoscale* **9**, 10992-10997 (2017).
121. T. Zhang, X. Chen, Y. Thakur, B. Lu, Q. Zhang, J. Runt, Q. M. Zhang, A highly scalable dielectric metamaterial with superior capacitor performance over a broad temperature. *Science Advances* **6**, eaax6622 (2020).
122. L. Li, J. Cheng, Y. Cheng, T. Han, Y. Liu, Y. Zhou, G. Zhao, Y. Zhao, C. Xiong, L. Dong, Q. Wang, Significant improvements in dielectric constant and energy density of ferroelectric polymer nanocomposites enabled by ultralow contents of nanofillers. *Advanced Materials* **33**, 2102392 (2021).
123. C.-W. Nan, M. Bichurin, S. Dong, D. Viehland, G. Srinivasan, Multiferroic magnetoelectric composites: Historical perspective, status, and future directions. *Journal of Applied Physics* **103**, 031101 (2008).
124. K. Zou, C. Shao, P. Bai, C. Zhang, Y. Yang, R. Guo, H. Huang, W. Luo, R. Ma, Y. Cao, Giant room-temperature electrocaloric effect of polymer-ceramic composites with orientated BaSrTiO3 nanofibers. *Nano Letters* **22**, 6560-6566 (2022).
125. M.-D. Li, X.-Q. Shen, X. Chen, J.-M. Gan, F. Wang, J. Li, X.-L. Wang, Q.-D. Shen, Thermal management of chips by a device prototype using synergistic effects of 3-D heat-conductive network and electrocaloric refrigeration. *Nature Communications* **13**, 5849 (2022).
126. G. Qian, K. Zhu, X. Li, K. Yan, J. Wang, J. Liu, W. Huang, The electrocaloric effect of PBZ/PVDF flexible composite film near room temperature. *Journal of Materials Science: Materials in Electronics* **32**, 12001-12016 (2021).
127. Z. Wang, Y. Gao, Y. Ma, X. Xie, M. Yang, H. Zhang, Enhanced electrocaloric effect within a broad temperature range in lead-free polymer composite films by blending the rare-earth doped BaTiO 3 nanopowders. *Advanced Composites and Hybrid Materials* **4**, 469-477 (2021).
128. P. Bai, Q. Zhang, H. Cui, Y. Bo, D. Zhang, W. He, Y. Chen, R. Ma, An active pixel‐matrix electrocaloric device for targeted and differential thermal management. *Advanced Materials*, 2209181 (2023).

ACKNOWLEDGEMENTS

Funding: Q.M.Z and X.C acknowledge the support from the U. S. Office of Naval Research under award number N00014-19-1-2028. X.Q. thanks National Natural Science Foundation of China (52076127), Natural Science Foundation of Shanghai (20ZR1471700, 22JC1401800) and the State Key Laboratory of Mechanical System and Vibration (Grant No. MSVZD202211). L.Z. acknowledges financial support from the US National Science Foundation (DMR-2103196).

Author contributions: Q.M.Z., X.Q., and X.C. wrote the manuscript and prepared figures. L.Z. revised and edited the manuscript.

Competing interests: Q.M.Z. and X.C. have filed a PCT Patent Application No. PCT/US2022/032214 at Penn State on the EM tetrapolymers and related EM devices. X.Q. has a patent application No WO/2022/257747 on the tetrapolymers and ECE. L.Z. has no competing interests.